ACADEMIC PRESS

Available online at www.sciencedirect.com
SCIENCE DIRECT®

NeuroImage

NeuroImage 20 (2003) 1848–1856

www.elsevier.com/locate/ynimg

Assessment of the impact of model-based scatter correction on [^{18}F]-FDG 3D brain PET in healthy subjects using statistical parametric mapping

Marie-Louise Montandon, Daniel O. Slosman, and Habib Zaidi*

Division of Nuclear Medicine, Geneva University Hospital, CH-1211 Geneva 4, Switzerland

Received 30 April 2003; revised 10 July 2003; accepted 21 July 2003

Abstract

It is recognized that scatter correction can supply more accurate absolute quantification, and that iterative reconstruction results in better noise properties and significantly reduces streak artefacts; however, it is not entirely clear whether they produce significant changes in [^{18}F]-FDG distribution of reconstructed 3D brain PET images relative to not scatter corrected images and analytic reconstruction procedures. The current study assesses the effect of model-based scatter correction using the single-scatter simulation algorithm and iterative reconstruction in 3D brain PET studies, using statistical parametric mapping (SPM) analysis. The study population consisted of 14 healthy volunteers (6 males, 8 females; age 63–80 years). PET images were reconstructed using an analytic 3DRP reprojection algorithm with (SC) and without explicit scatter correction (NSC), as well as using an iterative ordered subset–expectation maximization (OSEM) algorithm. Calculated attenuation correction was performed assuming uniform attenuation ($\mu = 0.096$ cm^{-1}) for brain tissues when data are precorrected for scatter. The broad-beam attenuation coefficient ($\mu = 0.06$ cm^{-1}) determined from phantom studies was applied to NSC images. The images were coregistered and normalized using the default [^{15}O]-H_2O template supplied with SPM99 and an [^{18}F]-FDG template. A *t* statistic image for the contrast condition effect was then constructed. The contrast comparing SC to NSC images suggest that regional brain metabolic activity decreases significantly in the frontal gyri, in addition to the middle temporal and postcentral gyri. On the other hand, activity increases in the cerebellum, thalamus, insula, brainstem, temporal lobe, and the frontal cortex. No significant changes were detected when comparing images reconstructed using analytic and iterative algorithms. It is concluded that, for some cerebral areas, significant differences in [^{18}F]-FDG distribution arise when images are reconstructed with and without explicit SC. This needs to be considered when interpreting [^{18}F]-FDG 3D brain PET images after applying SC.

Keywords: PET; Scatter correction; Brain imaging; Statistical parametric mapping

Introduction

In a clinical setting, the diagnosis of cerebral pathologies is generally based on qualitative assessment of the distribution pattern of specific tracers in molecular neuroimaging. On the other hand, the quantitative analysis of brain function using position emission tomography (PET) has made significant progress during the last few years due to improvements in PET instrumentation design and the development of sophisticated software tools to improve the quantitative accuracy and statistical analysis of PET data. Convincing clinical evaluations and research investigations based on PET imaging are providing clinicians with relevant functional information on various pathologies, and are serving as powerful tools to neuroscientists seeking advanced insight into the working of the human brain.

Still, the quantitative analysis of 3D brain PET images remains hampered by several physical factors, the most important being photon attenuation, contributions from scattered photons, and partial volume effects (Zaidi and Sossi, 2003). Moreover, scatter correction is of paramount importance in high resolution brain PET imaging, in which the scatter degradation features become more complex.

* Corresponding author. Fax: +41-22-372-7169.
E-mail address: habib.zaidi@hcuge.ch (H. Zaidi).

1053-8119/$ – see front matter © 2003 Elsevier Inc. All rights reserved.
doi:10.1016/j.neuroimage.2003.07.013

Much worthwhile effort has been spent addressing the scatter correction problem, which has led to the proposal of several algorithms with varying degrees of success. Nevertheless, none of them has proved to be sufficiently robust and accurate, thus spurring further efforts in this direction. Previous evaluations of scatter correction techniques have been limited to conventional qualitative assessment using clinical studies or quantitative regions of interest based analysis of Monte Carlo simulation or experimental phantom measurements (Zaidi, 2001). In addition to these evaluations, it is also desirable to investigate the effect of scatter correction on the distribution pattern of regional brain metabolic activity using realistic source distributions through voxel-based analysis techniques.

Statistical Parametric Mapping (SPM) (Wellcome Department of Cognitive Neurology, University College London, UK) is among the state-of-the-art packages for statistical analysis of neuroimaging data because it is very flexible, well documented, and extensively tested (Friston et al., 1999). Using SPM and SPECT data of normal subjects reconstructed with the triple-energy window scatter correction method and without explicit scatter correction but partially compensated using an effective linear attenuation coefficient, Shiga et al. (2002) demonstrated that differences in the ^{123}I-IMP distribution arise in different cerebral structures when the data are processed using both protocols. These differences could potentially cause reduced diagnostic accuracy and false interpretation of images. In a related study, Matsuda et al. (2002) compared reduction in regional cerebral blood flow (rCBF) in patients with probable Alzheimer's disease before and after correction for partial volume effects. They concluded that this correction is essential for investigation of the atrophied brain when using SPECT cameras with limited spatial resolution. The current study assesses the effect of model-based scatter correction on the distribution of [^{18}F]fluorodeoxyglucose ([^{18}F]-FDG) in 3D brain PET studies using SPM analysis in healthy volunteers.

Materials and methods

Subjects

The study population consisted of 17 right-handed healthy volunteers. This limited set of subjects was recruited within the framework of the NRP38 program (Slosman et al., 2001), which is a large project focusing on early diagnosis of dementia of Alzheimer's type. This study was approved by the ethics committee of Geneva University Hospital, and all healthy volunteers gave their written informed consent for participation. The 17 subjects were randomly drawn from the larger pool of healthy volunteers; 3 of them were excluded because of insufficient image quality, technical failure, or pathological findings. The remaining 14 normal subjects (6 males, 8 females) were used in this study. Their age ranged from 63 to 80 years (mean $\pm$ SD = 70.6 $\pm$ 4.8 years).

PET data acquisition and reconstruction

PET data acquisition (25 min) started 30 min after intravenous injection of approximately 300 MBq of [^{18}F]-FDG on the ECAT ART continuously rotating partial-ring positron tomograph (CTI/Siemens, Knoxville, TN), operated in fully 3D mode. Images were first reconstructed using an analytic 3DRP reprojection algorithm (Kinahan and Rogers, 1989) with (SC) and without explicit scatter correction (NSC). The default parameters used in clinical routine were applied (Ramp filter, cut-off frequency 0.35 cycles/pixel). In a second step, the scatter corrected data sets were reconstructed by means of a 2D iterative normalized attenuation weighted, ordered subset–expectation maximization reconstruction (NAW OSEM) following Fourier rebinning (FORE) (Michel et al., 1998). In FORE, oblique rays are binned to a transaxial slice using the frequency-distance relationship of the data in Fourier space. This algorithm rebins the 3D data into a stack of ordinary 2D direct sinograms and the image is reconstructed in 2D slice-by-slice. The OSEM reconstruction parameters were 6 iterations and 16 subsets followed by a postprocessing Gaussian filter (kernel FWHM = 6.0 mm). The reconstructed images consist of 47 slices with 128 $\times$ 128 resolution and a voxel size set to 1.72 $\times$ 1.72 $\times$ 3.4 mm^3.

Attenuation and scatter corrections

Scatter correction was performed using a model-based scatter correction algorithm that combines both the emission scan and attenuation map together with the physics of Compton scattering to estimate the scatter distribution (Watson et al., 1997). Calculated attenuation correction was performed by approximating the outline of the head using a slice-dependent ellipse assuming uniform attenuation for brain tissues. The narrow-beam linear attenuation coefficient (μ = 0.096 cm^{-1}) was used for scatter corrected data sets, while a broad-beam coefficient (μ = 0.06 cm^{-1}) determined from phantom studies as explained below was applied to noncorrected images to partially compensate the contribution from scattered photons and the resulting overcorrection for attenuation effect. A slightly lower value of the attenuation coefficient is used for the following reason (Zaidi and Montandon, 2002). The full value of μ predicts how many photons will be removed from a single, narrow-beam of radiation due to the combined processes of absorption and scatter. It ignores the number of photons that can be scattered into the path from other directions. That is, it ignores the build-up caused by the broad-beam conditions of nuclear medicine imaging. Use of the actual narrow-beam value of μ without explicitly correcting for scatter will overcorrect for attenuation and an image excessively hot in the center will result. Although images may be cos-

metically enhanced, improvements in image quantitation are only minimal with the reduced μ method of scatter correction. This is because this method assumes that scatter affects all locations in the image to the same extent. However, scatter is object and depth dependent, and a correction method that does not take this fact into account may result in large quantitation errors.

The determination of the effective linear attenuation coefficient for 511 keV photons was carried out following the approach originally proposed by Stodilka et al. (1998) and used by Van Laere et al. (2000) for determining an empiric optimal attenuation coefficient for 140 keV in brain SPECT imaging. The method entailed the following steps: the external cylinder supplied with the commercial 3D Hoffman brain phantom (Data Spectrum Corporation, Hillsborough, NC) was homogeneously filled with [^{18}F]-FDG to simulate typical brain imaging conditions. Uniform attenuation maps were constructed by manually fitting a circular region of interest on all slices containing the cylinder, followed by assignment of a constant attenuation coefficient varying between 0.04 and 0.1 cm^{-1}. Horizontal and vertical count profiles through the reconstructed cylinder (averaged over the central 10 pixels) were then determined and fitted to pixel position (x) along the profile (p) assuming symmetric quadratic distribution of the form $p(x) = a\,x^2 + b$. The coefficient b reflects the capacity of uniform attenuation correction to yield uniform profiles, that is $b = 0$ at the optimal effective attenuation coefficient μ_{eff}. This latter was estimated through quadratic interpolation from the experimental (μ_i, b_i) pairs (Van Laere et al., 2000). Consistent with results obtained by Cherry et al. (1991), the optimal effective μ value in 3D brain imaging is much lower compared to the theoretical value for scatter corrected data (μ = 0.096 cm^{-1}) and was found to be equal to 0.06 cm^{-1}.

Spatial normalization and statistical analysis

SPM is now considered among the gold standard tools and is being used worldwide both in research and clinical neuroimaging investigations. It consists in the construction of spatially extended statistical processes to tests hypotheses regarding regionally specific effects in neuroimaging (Friston et al., 1995; Worsley et al., 1996). The steps involved in the statistical analysis of brain PET images include: coregistration, spatial normalization, Gaussian smoothing, and construction of statistical parametric maps. The images were coregistered and normalized using SPM99 (Friston et al., 1999). A voxelwise unpaired t test was performed generating a t statistic map with 26 degrees of freedom for the contrast condition effect after to specification of a design matrix. This was then converted to a Z map to assess statistical significance at a P level of 0.05 corrected for multiple comparisons. Changes in regional cerebral glucose metabolism produced by two different conditions: (1) SC vs. NSC and (2) analytic 3DRP vs. iterative OSEM reconstructions, were investigated according to the general linear model in each voxel. Proportional scaling was applied by adjusting the mean global activity of each scan to 50 ml/100 ml/min and the threshold of gray matter to 0.80. A voxel-level threshold of 0.001 corrected for multiple comparisons was used. Spatial normalization is among the most important preprocessing steps in SPM analysis. Since MR images of the subjects were unavailable, we were limited to functional templates. Two templates were used for spatial normalization: (1) the standard PET template provided with SPM99 initially constructed at the Wellcome Department of Cognitive Neurology (University College London, UK) using [^{15}O]-H_2O PET images of 12 normal subjects scanned in resting condition with eyes closed, and (2) a specially designed [^{18}F]-FDG PET template constructed at Gregorio Marañón University Hospital (Madrid, Spain) by scanning 17 normal subjects in resting condition with eyes open during tracer uptake in a dark room (Gispert et al., 2003). This template was built by averaging [^{18}F]-FDG PET images normalized to the [^{15}O]-H_2O template followed by Gaussian smoothing (8 mm) according to the approach used by Signorini et al. (1999). It is worth emphasizing that the default SPM99 template is commonly applied regardless of the specificities of the tracer being used and subjects' conditions. Fig. 1 illustrates the standard [^{15}O]-H_2O supplied with SPM99 software package and the [^{18}F]-FDG template used in this study.

Results

Fig. 2 shows brain images with good statistics of a healthy volunteer as reconstructed by 3DRP after model-based scatter correction, the same analytic reconstruction algorithm without explicit scatter correction, and the iterative OSEM reconstruction algorithm, respectively. Horizontal profiles drawn through the thalamus of this slice are also illustrated. Model-based scatter correction significantly improved image quality and overall contrast between brain structures at the expense of a poor signal-to-noise ratio (Zaidi, 2000) as demonstrated on the mean images of the healthy volunteers (Fig. 3). It has also been shown that iterative OSEM reconstructions produce good quality images that have better signal-to-noise ratio, especially when an efficient regularization scheme is used to account for the ill-posedness nature of the reconstruction problem. The mean images reconstructed using 3DRP with and without explicit scatter correction together with difference maps calculated as mean(SC) − mean(NSC) and mean(NSC) − mean(SC) are shown in Fig. 3 to better illustrate the differences between reconstructing the same data with SC and NSC, while avoiding problems of interpreting significance due to an artificially low variance estimate since only one scan per subject were acquired.

Table 1 lists the peaks of the most significant decreases and increases in brain metabolism when images are normalized using both the default [^{15}O]-H_2O template supplied

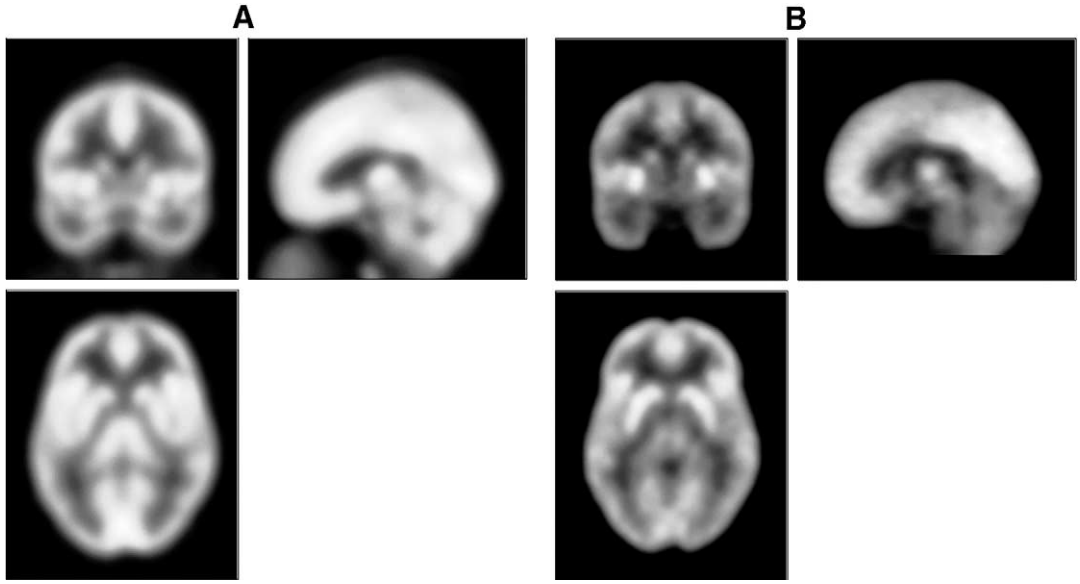

Fig. 1. Illustration of default [^{15}O]-H_2O template supplied with SPM99 software package (A) and [^{18}F]-FDG template (B) constructed by averaging [^{18}F]-FDG PET images of 17 normal subjects normalized to the standard [^{15}O]-H_2O PET template (Gispert et al., 2003).

with SPM99 and the tracer-specific [^{18}F]-FDG template, respectively. The brain structures were determined from the stereotactic coordinates with respect to the Talairach and Tournoux atlas (Talairach and Tournoux, 1988). Algebraic values of the scores are also shown (− = decrease, + = increase). Fig. 4 illustrates the areas with significant changes in brain metabolism obtained by comparing distributions with and without explicit SC normalized using the same template. The results obtained when comparing SC to NSC images suggest that [^{18}F]-FDG distribution decreases essentially in the frontal gyri, but also in the superior temporal, supramarginal, and middle occipital gyri. In contrast, the distribution increases mainly in the cerebellum, brainstem, insula, and putamen when comparing SC to NSC. Similarly, areas with significant decreases and increases in brain metabolism resulting from the comparison of SC and NSC images normalized using the same template are shown in Fig. 5. The results obtained when comparing SC to NSC images suggest that [^{18}F]-FDG distribution decreases significantly in the frontal gyri, in addition to the middle temporal and postcentral gyri. On the other hand, the distribution increases in the cerebellum, thalamus, insula, the brainstem, temporal lobe, and the frontal cortex when comparing SC to NSC. As expected, there are no significant changes between images reconstructed using analytic and iterative reconstruction algorithms.

Discussion

It is generally well accepted that scatter correction improves the contrast between brain structures and can supply more accurate absolute quantification. Iterative reconstruction is also recognized to significantly reduce streak artefacts and produce less noisy images. However, it is not entirely clear whether either scatter correction or iterative reconstruction produce significant changes in [^{18}F]-FDG distribution of 3D brain PET images compared to images not explicitly corrected for scatter or reconstructed using an analytic algorithm, respectively. Over the last two decades, several algorithms have been developed for reducing the degradation of image contrast and loss of quantitative accuracy resulting from scatter events during data collection. Different versions of these methods have been successfully implemented for 3D PET. The main difference among the correction methods is the way in which the scatter component is estimated (Zaidi, 2000). The major drawback of subtraction-based scatter correction is the increase in statistical noise. In this respect, iterative statistical reconstruction-based scatter correction methods have better noise properties, which make them particularly suited to low-count emission studies. However, such methods are time consuming and costly and hence not yet practical for clinical routine applications (Zaidi, 2001). The advantages of iterative reconstruction algorithms over analytic methods were recently investigated in PET activation studies (Reinders et al., 2002). It has been shown that iterative OSEM produces fewer false-positive clusters and has the potential to increase the statistical power in PET activation studies compared with analytic reconstruction provided balanced subsets hold and sufficient number of iterations are used to obtain full convergence.

The contribution of scatter correction toward improved quantitative [^{18}F]-FDG PET imaging is well established. However, its application in [^{15}O]-H_2O activation studies

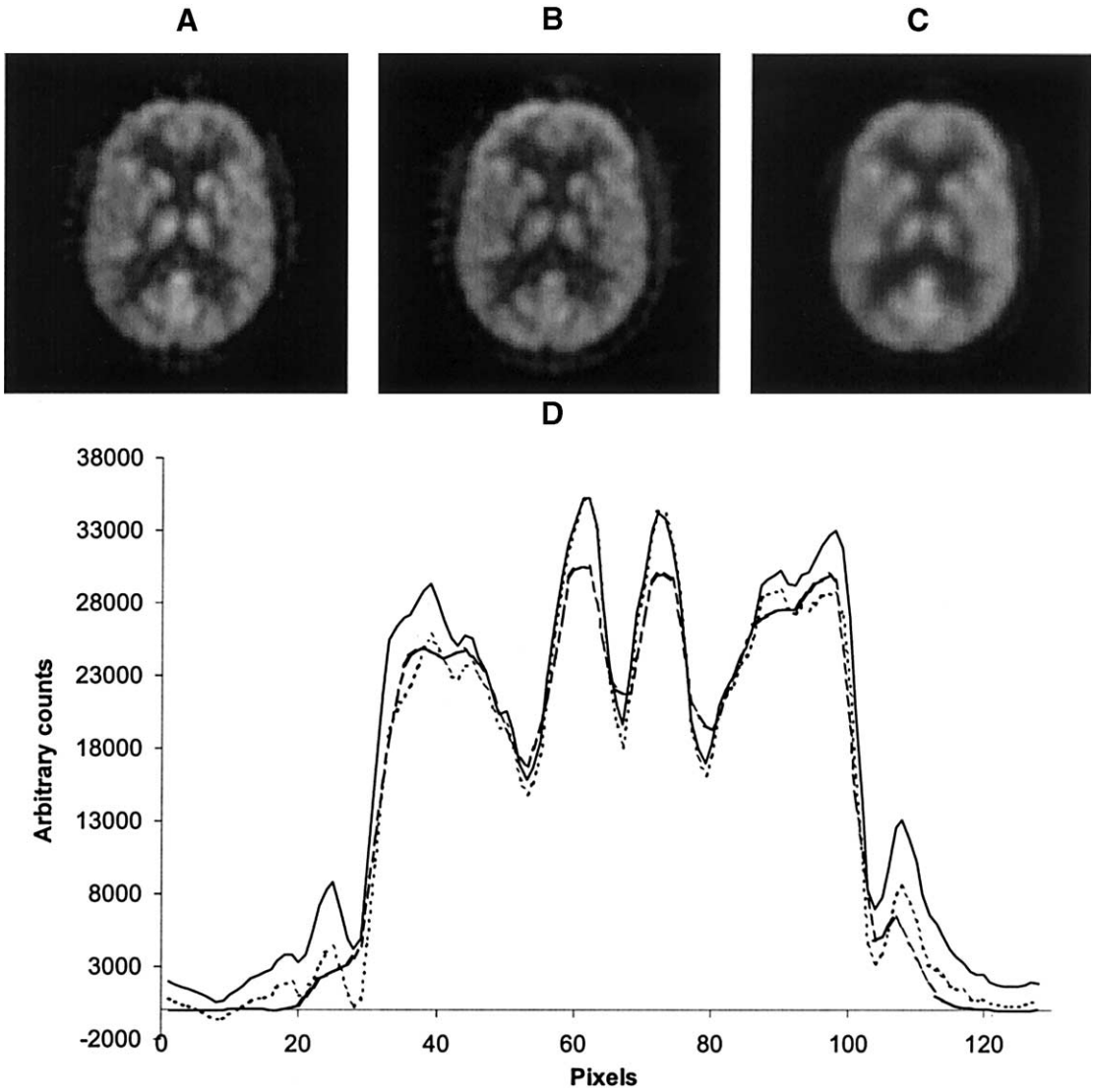

Fig. 2. Typical brain images of a healthy volunteer obtained using model-based scatter correction and analytic 3DRP reconstruction (A), attenuation correction using an effective linear attenuation coefficient ($\mu = 0.06$ cm^{-1}) to partially compensate for scatter contribution (B), and model-based scatter correction followed by iterative OSEM reconstruction (C). Comparison of horizontal profiles between images reconstructed using 3DRP without (solid line) and with (dotted line) scatter correction as well as iterative OSEM (shaded line) reconstruction algorithm (D).

suffering from low-count statistics is still controversial in view of the fact that scatter correction will increase the spatial specificity by decreasing the bias at the cost of increased variance. Obviously the sensitivity of SPM analysis will be influenced by the poor signal-to-noise ratio of PET images reconstructed after scatter subtraction, therefore decreasing the statistical power of activation studies. Van Laere et al. (2002) reported that absence of scatter correction resulted in an increase in minimally detectable activation and that this effect is definitely the largest factor that decreases the sensitivity of SPM analysis, more than resolution or reconstruction procedure. In this study, we focused on the impact of model-based scatter correction using the single-scatter simulation algorithm for estimation of the scatter component (Watson et al., 1997) using SPM analysis. Our work is closely related to the recent study performed by Shiga et al. (2002) using brain SPECT images and the triple energy window method for scatter correction. Their results provided evidence for the effect of scatter correction on regional distribution of ^{123}I-IMP, stimulating further research using other tracers and imaging modalities. In addition, we also examined the effect of the normalization template on the outcome of statistical parametric mapping. Consistent with the conclusions drawn from the study by Gispert et al. (2003), our results demonstrate that the inappropriate use of the standard template supplied with SPM99 can lead to inconsistent results, since the areas differed significantly between using the standard [^{15}O]-H_2O template supplied with SPM99 software package and the specific [^{18}F]-FDG template. The limitations of SPM with respect to the accuracy and sensitivity of quantitative analysis have been addressed elsewhere using realistic Monte

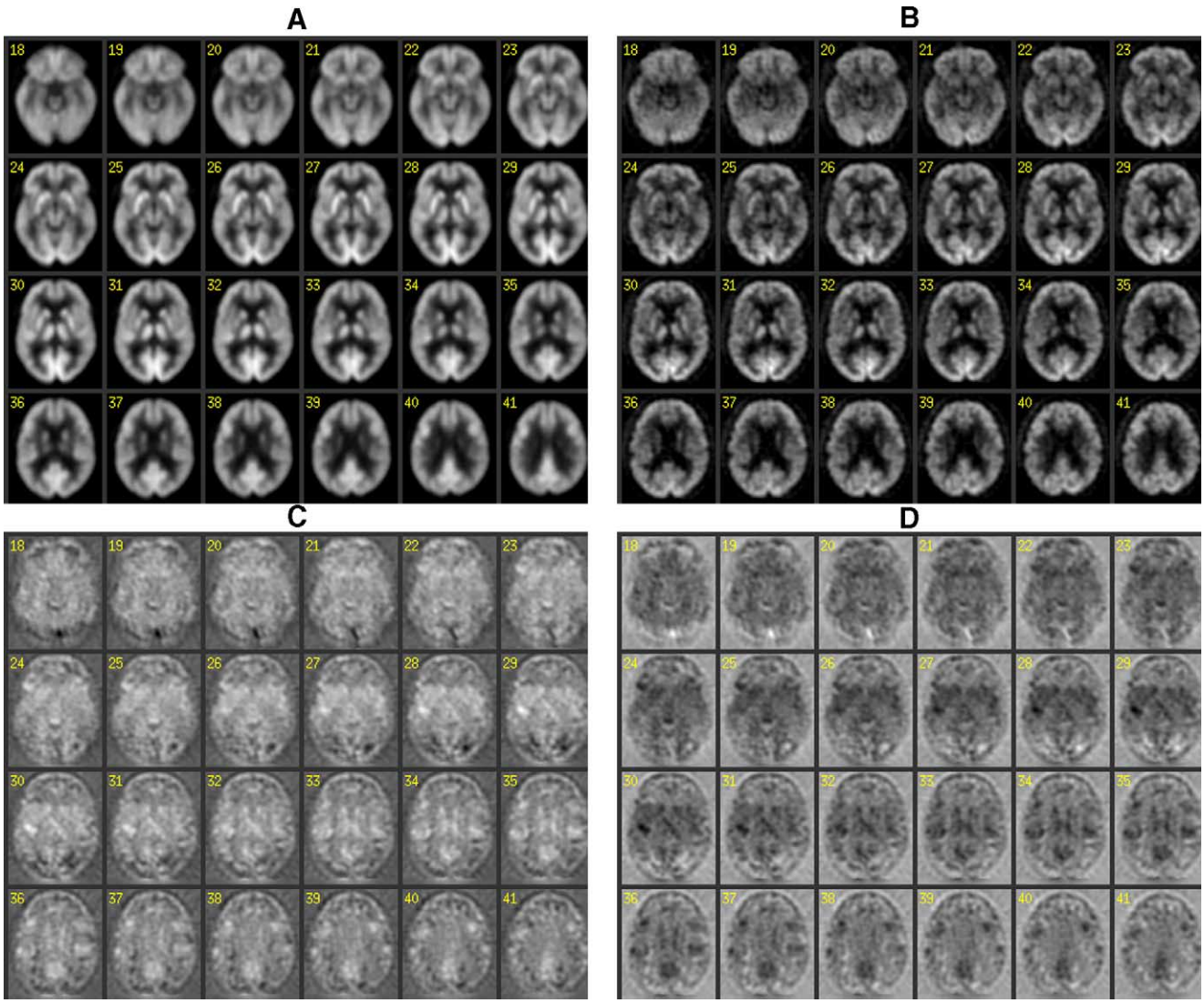

Fig. 3. Mean [^{18}F]-FDG PET images of normal subjects reconstructed using analytic 3DRP algorithm with (A) and without (B) explicit scatter correction. The window level was set to interval 20–100%. The raw difference maps generated by subtracting A minus B (C) and B minus A (D) are also shown.

Carlo simulated data incorporating accurate modelling of the physical processes involved in PET data acquisition (Schoenahl et al., 2003).

In agreement with the observations made in previous studies (Bailey, 1998; Zaidi, 2000), an analysis of the difference images between noncorrected and scatter-corrected data revealed the regional effect of scatter correction. In particular, they look like attenuation corrected images, especially the contrast between the brain tissue and the air-filled sinuses. In addition, the physics of photon interactions indicates that in a low density region, the amount of scattering is negligible. However, many incorrectly positioned events will be assigned to projection data through the low density region with similar probabilities to an adjacent, more dense region, as a result of the coincidence detection method (Bailey, 1998). This is a possible explanation for the fact that the presence of a small, low density region will hardly be visible on the scatter profile in the projection data. The resulting effect after reconstruction is the underestimation of scatter contribution from this region.

A clinical diagnosis is generally accomplished based on the distribution pattern of regional brain metabolic activity. Cerebral pathologies such as cerebrovascular disorders, brain trauma, epilepsy, neurodegenerative disorders, and Parkinson's disease, and mental disorders such as depression, schizophrenia, and obsessive-compulsive disorders are known to result in regional glucose consumption abnormalities (Kim et al., 2002; Slosman et al., 2001; Gispert et al., 2003; Piert et al., 1996; Berding et al., 2001). Decreased brain metabolism in frontal areas and occasionally in temporal and parietal cortices has also been observed in normal aging (Loessner et al., 1995). Our voxel-based analysis revealed statistically significant differences between PET images reconstructed using SC and NSC. Therefore, knowledge of these differences is highly desired for continuing adequate reading of 3D brain PET images by nuclear phy-

Table 1
Results of statistical analysis comparing images reconstructed with model-based scatter correction to those corrected for attenuation using an effective linear attenuation coefficient without explicit scatter correction normalized using the default [^{15}O]-H_2O template supplied with SPM99 software package and the tracer-specific [^{18}F]-FDG template[a]

Cerebral structure	*Z* score using [^{5}O]-H_2O template	*Z* score using [^{18}F]-FDG template	Algebraic value
Right middle frontal gyrus	6.42	6.07	−
Right supramarginal gyrus	5.73	—	−
Right middle occipital gyrus	5.57	—	−
Right superior frontal gyrus	5.33	—	−
Right superior temporal gyrus	5.27	—	−
Right superior frontal gyrus	4.85	4.80	−
Left medial frontal gyrus	4.80	—	−
Right middle frontal gyrus	—	6.07	−
Right middle temporal gyrus	—	5.43	−
Right postcentral gyrus	—	5.37	−
Right superior frontal gyrus	—	5.26	−
Left precentral gyrus	—	4.83	−
Right medulla	6.50	—	+
Left cerebellum	6.38	—	+
Right midbrain	6.05	—	+
Left frontal lobe	5.78	—	+
Right putamen	5.76	—	+
Left insula	5.46	5.67	+
Left temporal lobe	5.46	—	+
Right cerebellum	—	6.75	+
Right thalamus	—	6.13	+
Right medulla	—	5.59	+
Left rectal gyrus	—	5.57	+
Left temporal lobe	—	5.13	+
Right inferior frontal gyrus	—	5.08	+

[a] The cerebral structure corresponding to areas of significant regional decreases (−) and increases (+) in brain metabolism (highest *Z* score) determined from the Talairach coordinates are shown.

sicians accustomed to interpreting images reconstructed using a specific processing protocol (e.g., without explicit scatter correction) after software upgrades incorporating modifications in image correction techniques. It is likely that understanding the effects of scatter correction would assist in minimizing the risk of misdiagnosis. The results obtained might be different, however, when dealing with patients exhibiting abnormal distribution patterns. Further research in this direction is guaranteed.

It is concluded that significant differences in regional brain metabolic activity distribution arise when images are reconstructed with and without explicit SC for some cerebral areas. This needs to be considered for adequate interpretation of [^{18}F]-FDG 3D brain PET images after applying

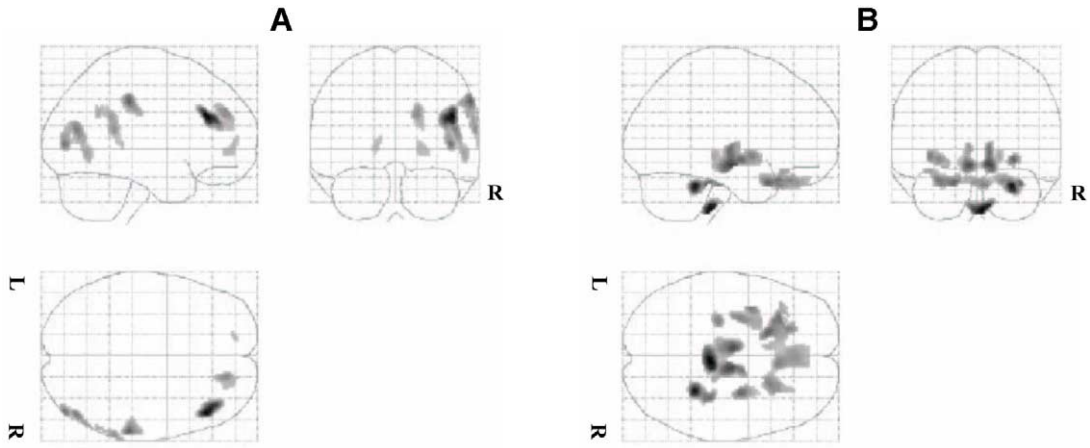

Fig. 4. Statistical parametric maps resulting from the comparison of images reconstructed using model-based scatter correction and those corrected for attenuation using an effective linear attenuation coefficient without explicit scatter correction normalized using the standard [^{15}O]-H_2O template supplied with SPM99, showing areas of significant regional decreases (A) and increases (B) in brain metabolism.

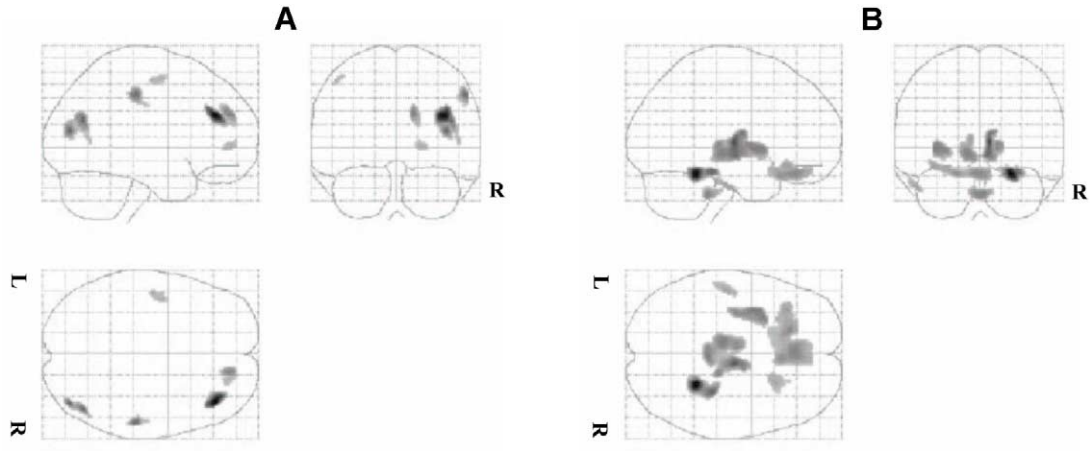

Fig. 5. Statistical parametric maps resulting from the comparison of images reconstructed using model-based scatter correction and those corrected for attenuation using an effective linear attenuation coefficient without explicit scatter correction normalized using the [^{18}F]-FDG template showing areas of significant regional decreases (A) and increases (B) in brain metabolism.

scatter correction associated with software upgrades or modifications of processing protocols.

Acknowledgments

The authors thank both reviewers for very thoughtful and helpful suggestions that greatly improved the quality of the manuscript. This work was supported by the Swiss National Science Foundation under grant SNSF 3152-062008 and 3152A0-102143, and the Department of Radiology, Geneva University Hospital. The authors would like to thank Juan D. Gispert for supplying the [^{18}F]-FDG template.

References

Bailey, D.L., 1998. Quantitative procedures in 3D PET, in: Bendriem, B., Townsend, D.W. (Eds.), The Theory and Practice of 3D PET, Kluwer Academic Publishers, Dordrecht, pp. 55–109.

Berding, G., Odin, P., Brooks, D.J., et al., 2001. Resting regional cerebral glucose metabolism in advanced Parkinson's disease studied in the off and on conditions with [(18)F]FDG-PET. Mov. Disord. 16, 1014–1022.

Cherry, S.R., Dahlbom, M., Hoffman, E.J., 1991. 3D PET using a conventional multislice tomograph without septa. J. Comput. Assist. Tomogr. 15, 655–668.

Friston, K., Ashburner, J., Heather, J., et al., 1999. "Statistical Parametric Mapping." Available at: www.fil.ion.ucl.ac.uk/spm (The Wellcome Department of Cognitive Neurology, University College London, London).

Friston, K., Holmes, A., Worsley, K., et al., 1995. Statistical parametric maps in functional imaging: a general linear approach. Hum. Brain Mapp. 2, 189–210.

Gispert, J.D., Pascau, J., Reig, S., et al., 2003. Influence of the normalization template on the outcome of statistical parametric mapping of PET scans. NeuroImage 18, 601–612.

Kim, Y.K., Lee, D.S., Lee, S.K., et al., 2002. ^{18}F-FDG PET in localization of frontal lobe epilepsy: comparison of visual and SPM analysis. J. Nucl. Med. 43, 1167–1174.

Kinahan, P.E., Rogers, J.G., 1989. Analytic 3D image reconstruction using all detected events. IEEE Trans. Nucl. Sci. 36, 964–968.

Loessner, A., Alavi, A., Lewandrowski, K.U., et al., 1995. Regional cerebral function determined by FDG-PET in healthy volunteers: normal patterns and changes with age. J. Nucl. Med. 36, 1141–1149.

Matsuda, H., Kanetaka, H., Ohnishi, T., et al., 2002. Brain SPET abnormalities in Alzheimer's disease before and after atrophy correction. Eur. J. Nucl. Med. Mol. Imaging 29, 1502–1505.

Michel, C., Sibomana, M., Boi, A., et al., 1998. Preserving poisson characteristics of PET data with weighted OSEM reconstruction, in: Proceedings of the IEEE Nuclear Science Symposium and Medical Imaging Conference, IEEE, Toronto, Canada, pp. 1323–1329.

Piert, M., Koeppe, R.A., Giordani, B., et al., 1996. Diminished glucose transport and phosphorylation in Alzheimer's disease determined by dynamic FDG-PET. J. Nucl. Med. 37, 201–208.

Reinders, A.A., Paans, A.M., de Jong, B.M., et al., 2002. Iterative versus filtered backprojection reconstruction for statistical parametric mapping of PET activation measurements: a comparative case study. NeuroImage 15, 175–181.

Schoenahl, F., Montandon, M.-L., Slosman, D., Zaidi, H., 2003. Assessment of the performance of SPM analysis in PET neuroactivation studies: a Monte Carlo investigation, in: Conference Proceedings of the VIIth International Meeting on Fully Three-dimensional Image Reconstruction in Radiology and Nuclear Medicine, 29 June–4 July 2003, Saint-Malo, France. Available at: http://dmnu-pet5.hcuge.ch.

Shiga, T., Kubo, N., Takano, A., et al., 2002. The effect of scatter correction on ^{123}I-IMP brain perfusion SPET with the triple energy window method in normal subjects using SPM analysis. Eur. J. Nucl. Med. 29, 342–345.

Signorini, M., Paulesu, E., Friston, K., et al., 1999. Rapid assessment of regional cerebral metabolic abnormalities in single subjects with quantitative and nonquantitative [18F]FDG PET: a clinical validation of statistical parametric mapping. NeuroImage 9, 63–80.

Slosman, D.O., Ludwig, C., Zerarka, S., et al., 2001. Brain energy metabolism in Alzheimer's disease: ^{99m}Tc-HMPAO SPECT imaging during verbal fluency and role of astrocytes in the cellular mechanism of ^{99m}Tc-HMPAO retention. Brain Res. Rev. 36, 230–240.

Stodilka, R.Z., Kemp, B.J., Prato, F.S., Nicholson, R.L., 1998. Importance of bone attenuation in brain SPECT quantification. J. Nucl. Med. 39, 190–197.

Talairach, J., Tournoux, P., 1988. Co-Planar Atlas of the Human Brain. Thieme Medical Publishers, New York.

Van Laere, K., Koole, M., Kauppinen, T., et al., 2000. Nonuniform transmission in brain SPECT using ^{201}T1, ^{153}Gd, and ^{99m}Tc static line

sources: anthropomorphic dosimetry studies and influence on brain quantification. J. Nucl. Med. 41, 2051–2062.

Van Laere, K.J., Versijpt, J., Koole, M., et al., 2002. Experimental performance assessment of SPM for SPECT neuroactivation studies using a subresolution sandwich phantom design. Neuroimage 16, 200–216.

Watson, C.C., Newport, D., Casey, M.E., et al., 1997. Evaluation of simulation-based scatter correction for 3-D PET cardiac imaging. IEEE Trans. Nucl. Sci. 44, 90–97.

Worsley, K.J., Marrett, S., Neelin, P., et al., 1996. A unified statistical approach for determining significant signals in images of cerebral activation. Hum. Brain Mapp. 4, 58–73.

Zaidi, H., 2000. Comparative evaluation of scatter correction techniques in 3D positron emission tomography. Eur. J. Nucl. Med. 27, 1813–1826.

Zaidi, H., 2001. Scatter modelling and correction strategies in fully 3D PET. Nucl. Med. Commun. 22, 1181–1184.

Zaidi, H., Montandon, M.-L., 2002. Which attenuation coefficient to use in combined attenuation and scatter corrections for quantitative brain SPET? Eur. J. Nucl. Med. 29, 967–969.

Zaidi, H., Sossi, V., 2003. Correction for image degrading factors is essential for accurate quantification of brain function using PET. Med. Phys. 30, In press.